SOFIA UNIVERSITY "ST. KLIMENT OHRIDSKI"

FACULTY OF CHEMISTRY AND PHARMACY

Department of Inorganic Chemistry

Martin Krastev Nedyalkov

INVESTIGATION OF THE INFLUENCE OF LANTHANIDE IONS ON SOME PHYSICAL PROPERTIES OF MW_2O_8 TYPE TUNGSTATES (M= Zr, Hf)

SYNOPSIS

of dissertation for awarding of

the educational and scientific degree "doctor"

in the professional field 4.2 Chemical Sciences

(Inorganic Chemistry)

Sofia, 2023

The dissertation contains 75 pages, includes scheme 1, tables 4, figures 21, references 78. Part of the results were published in two scientific papers. The dissertation was approbated by the Departmental Council of the Department of Inorganic Chemistry at the Faculty of Chemistry and Pharmacy of SU "St. Kliment Ohridski"on 30.01.2023.

Scientific supervisors: Prof. Dr. **Maria Milanova**, Assoc. Prof. Dr. **Martin Tsvetkov**

The thesis defense will take place on .... 2023 at .... in .... hall of the Faculty of Chemistry and Pharmacy, Sofia University, bul. Janes Bourchier, 1.

CONTENTS

INTRODUCTION

Over the past two decades, materials with a negative coefficient of thermal expansion (CTE) have become an intensely researched area. The discovery of materials exhibiting a negative CTE over a large temperature range, coupled with the elucidation of the mechanism determining this unusual property, was followed by predictions, that these materials will find application in various composite materials. These predictions make materials with a negative CTE attractive for science and practice. At the same time, in modern applications, materials with many specific properties are sought, including conductivity, magnetic and optical properties, hardness, ductility, etc., and this in turn complicates the achievement of zero or near-zero thermal expansion. In such cases, the use of composites is an alternative that can allow the preservation of the desired properties of the material, while improving the unwanted ones and acquiring new features. Materials with negative thermal expansion can theoretically be used to reduce or compensate for expansion by producing composites with controlled thermal expansion.

Potential applications of negative CTE materials in controlled thermal expansion composites range from coatings for optical fibers and electronics to dental fillings. Upon distension of road paves, railway tracks, bridges or thin layers, the incompatibilities in the thermal expansion of the components of the structure are a challenge to their assembly. Precise positioning is critical for electronic devices, and nanotechnology increases the control required for their operation.

Obtaining high-quality composites faces a number of challenges. There are limitations to the application of the various materials, one of which is related to the use of transition metals, which increases the cost of the materials. Problems have been identified affecting the stability of the materials in their processing conditions, as well as incompatibility with other composite components. These challenges are becoming areas of active research and efforts are directed at discovering new materials, improving the properties of existing ones, modifying them to achieve compatibility, and creating conditions for processing and obtaining homogeneous composites.

Research on the **modification of materials with lanthanide ions** in order to improve their properties is one of the scientific directions in the Laboratory of Chemistry of Rare Earth Elements in recent years. Studies conducted lately on the modification of titanium dioxide, zinc-nickel spinels, as well as mixed-metal oxides with a perovskite structure, clearly show the influence of lanthanide ions on the properties of the modified materials. The work on

modification of zirconium and hafnium tungstate with some lanthanide ions can be considered as a continuation of these studies. On the other hand, the literature review showed that it is the modification of these tungstates that is one of the ways to control their properties and lower their negative CTE and thus facilitate their potential application, e.g., in composite materials. The hydrothermal method for the synthesis of these compounds, pure and modified with lanthanide ions, has been applied in combination with instrumental methods for characterizing and establishing the changes in their physical properties.

The literature review in the field showed:

(i) the significance of zirconium and hafnium tungstate and their properties for their practical application in obtaining materials with negligible thermal expansion or low negative CTE;

(ii) the changes of basic characteristics and properties of these compounds, namely the unit cell parameter, the phase transition temperature, the coefficient of thermal expansion, as a result of modification with different ions;

(iii) limited research on the modification of zirconium and hafnium tungstate, mainly with a small number of triply- and quadruply-charged ions, due to difficulties in selecting ions to replace the quadruply-charged (Zr^{4+}/Hf^{4+}) and hexa-charged (W^{6+}) ions;

(iv) deficient research on the modification of zirconium and hafnium tungstate with lanthanide ions;

(v) considerably more intensive research on zirconium tungstate and much more restricted research on hafnium tungstate, with differences in the behavior of the two tungstates found mainly in studies on the effect of pressure on their properties;

(vi) research on the coefficient of thermal expansion of hydrothermally modified hafnium and zirconium tungstates is scanty or absent.

Assessment of the synthetic methods applied in the literature showed the advantages of the hydrothermal method for synthesis and modification of the studied tungstates, such as pathways to control the dosage of the modifying ion, characteristic of wet methods, and on the other hand, the possibility of calcining the samples at significantly lower temperature than in solid-phase synthesis.

Based on the literature review, **the aim** of the dissertation was set, namely to determine the changes in the structure and some physical properties of zirconium and hafnium tungstate, MW_2O_8 (M = Zr, Hf) as a result of their modification with lanthanide ions.

To achieve this goal, the following tasks **were set and completed**:

1. Synthesis of powder samples of ZrW_2O_8 and HfW_2O_8, pure and modified with lanthanide ions (Ln = Eu, Tb, Tm, Lu) by the hydrothermal method.

2. Characterization of the obtained samples by a set of instrumental methods, including high-temperature powder X-ray diffraction, Raman spectroscopy, transmission electron microscopy, scanning electron microscopy, infrared spectroscopy, UV/Vis absorption spectroscopy.

3. Determination of the coefficients of thermal expansion and phase transition temperature by high-temperature powder X-ray diffraction.

Ions with conmeasurable ionic radii, representatives of the medium, and heavy lanthanides, namely europium, terbium, thulium and lutetium, were selected for the modification. The selection of characterization methods is aimed at most exhaustive demonstration of the influence of lanthanide ions on the properties of zirconium and hafnium tungstate.
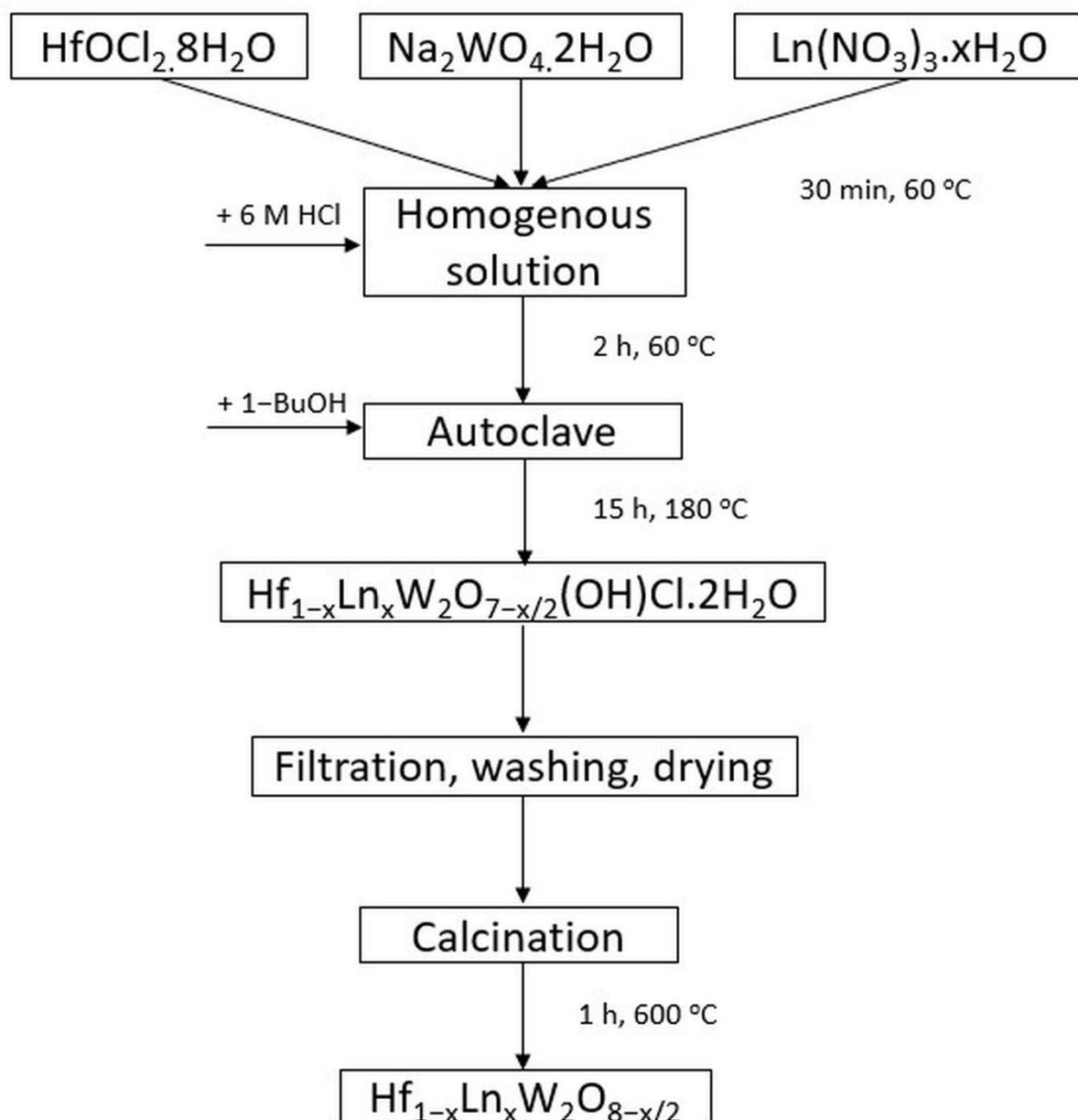
I. Synthetic procedure for the preparation of pure and lanthanide-modified zirconium and hafnium tungstate

The hydrothermal method was applied, the procedure being shown in Scheme 1. Salts of zirconium $ZrOCl_2 \cdot 8H_2O$/hafnium $HfOCl_2 \cdot 8H_2O$, and tungsten $Na_2WO_4 \cdot 2H_2O$, dissolved in deionized water were used. The solution was stirred at 60 °C for 30 min in a water bath. 6 M hydrochloric acid was added and stirred further for 2 h at 60 °C. Butyl alcohol was added to reduce the vapor pressure. The mixture was transferred to a "bomb" type autoclave, covered on the inside with Teflon, where it was stirred at a temperature of 180 °C for 15 h. The pressure was not controlled. An intermediate $MW_2O_7(OH)Cl \cdot 2H_2O$ was formed, which was washed with deionized water and dried at 50 °C. Zirconium tungstate is obtained by calcining the intermediate product $MW_2O_7(OH)Cl \cdot 2H_2O$ at 600 °C for 1 h [1].

The synthetic procedure is a modification of the procedure proposed by Liao *et al.* [2]. The changes concern *(i)* the heating conditions in the autoclave, namely the temperature and duration: the heating was carried out at a higher temperature but for a shorter time (180 °C, 15 h, instead of 130 °C, 24 h [2]), *(ii)* calcination. After filtration, washing, and drying, the

calcination of the samples was carried out at a temperature of 600 °C for 1 h instead of 30 min according to [2]. The change in procedure was necessitated by the discrepancy between our data and literature data obtained by the same procedure found in the initial experiments.

The synthesis of the modified samples followed the same scheme; the lanthanide nitrates were added to the initial solution.

$$HfOCl_2.8H_2O \qquad Na_2WO_4.2H_2O \qquad Ln(NO_3)_3.xH_2O$$

$+ 6 \text{ M HCl}$

30 min, 60 °C

Homogenous solution

2 h, 60 °C

$+ 1-BuOH$

Autoclave

15 h, 180 °C

$$Hf_{1-x}Ln_xW_2O_{7-x/2}(OH)Cl.2H_2O$$

Filtration, washing, drying

Calcination

1 h, 600 °C

$$Hf_{1-x}Ln_xW_2O_{8-x/2}$$

Scheme 1. Synthetic procedure for obtaining zirconium and hafnium tungstate – pure and modified with lanthanide ions

II. Solid solutions based on ZrW_2O_8 modified with Eu^{3+} and Tb^{3+}

II.1. Phase homogeneity of samples

High-temperature X-ray diffraction patterns for pure ZrW_2O_8 were taken in the range 25–250 °C and show phase homogeneity (Fig. 1). The Eu^{3+}- and Tb^{3+}-modified ZrW_2O_8 samples show good crystallinity and refletions matching those known in the literature for ZrW_2O_8 at 25 °C (Fig. 2, 3). They are also phase-homogeneous, with no additional phases containing W or Zr. The reflections in the X-ray pattern at 39.28 and 45.67 2θ are typical for Pt (111) and (002) and are due to the platinum substrate used during the measurements.
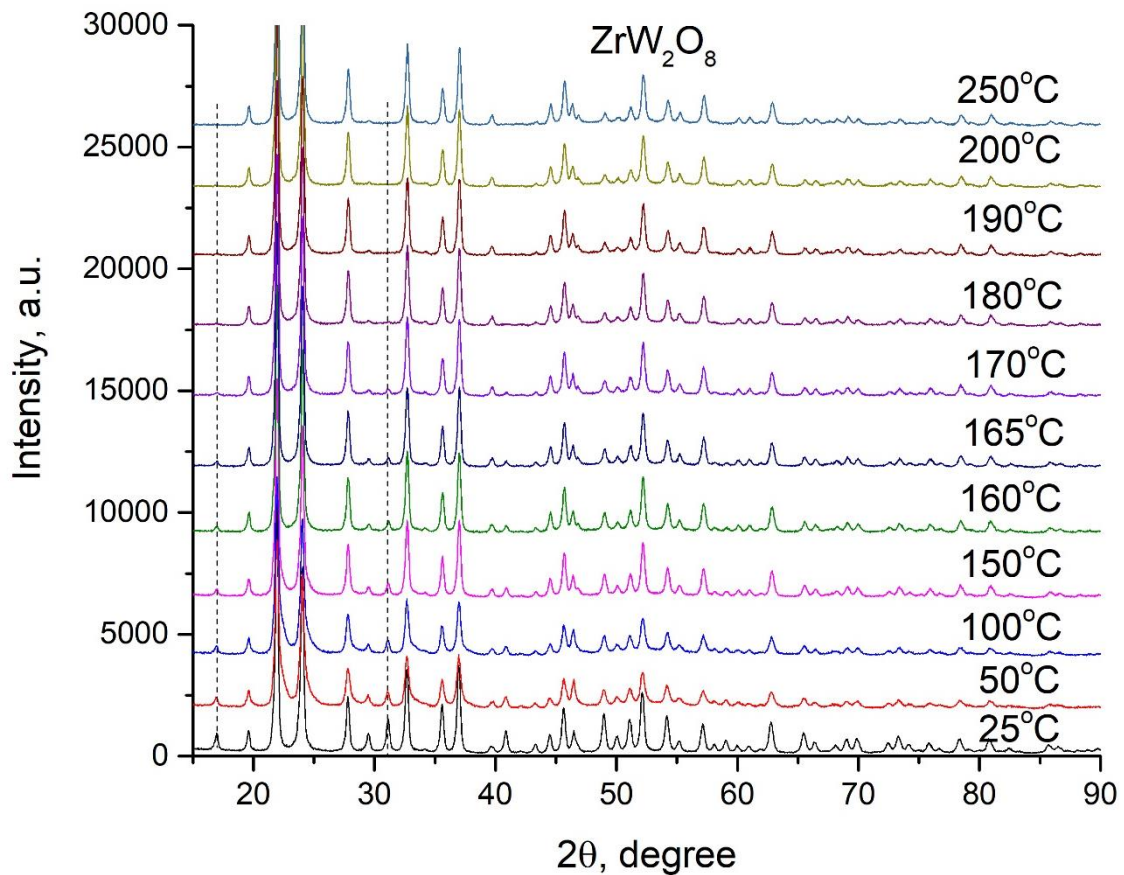

Figure 1. X-ray patterns of ZrW_2O_8 taken in the interval 25-250 °C

II.2. Phase transition α-ZrW_2O_8 → β-ZrW_2O_8

The phase transition α-ZrW_2O_8 → β-ZrW_2O_8 is monitored by a change in the intensity of the (110) and (310) reflections. These reflections are characteristic of the low-temperature α-ZrW_2O phase, but not of the high-temperature β-ZrW_2O_8. The dashed lines/ellipses (Fig. 1-3) show that with increasing temperature the intensity of these reflexes decreases and disappears

8

completely above the phase transition temperature. The change of the mentioned reflexes (110) and (310) is monitored, since they are the most intense. There are other reflexes that change with temperature, but they are of negligible intensity.
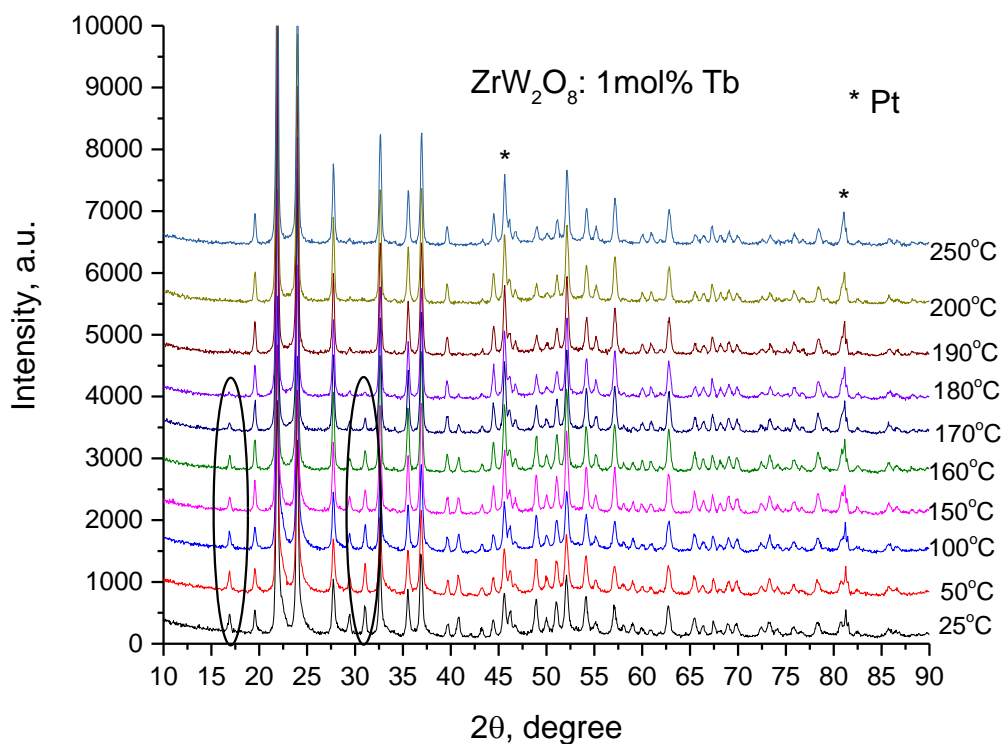

Figure 2. X-ray patterns of ZrW_2O_8 modified with 1 mol % terbium, 25–250 °C
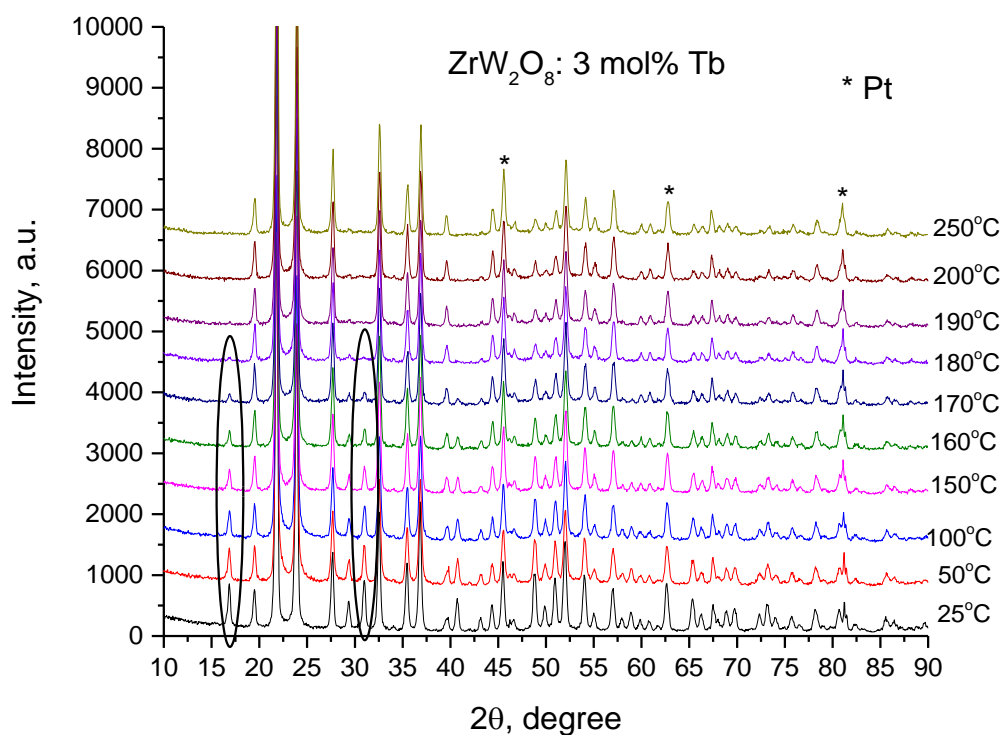

Figure 3. X-ray patterns of ZrW_2O_8 modified with 3 mol % terbium, 25–250 °C

The (310) reflection tracing in the high-temperature X-ray diffraction patterns shows that the modification of ZrW_2O_8 with Eu^{3+} causes an increase in the phase transition temperature (Fig. 4). For pure ZrW_2O_8 this temperature is 453 K (180 °C), while for the Eu^{3+}-modified one it is clearly higher. The absence of the (310) reflection in the diffraction pattern of the unmodified tungstate at 180 °C (453 K) is evidence of a complete conversion to the β-ZrW_2O_8 phase (Fig. 1, 4, 5). In the diffractograms of the modified with 1 and 2 mol % Eu^{3+} at this temperature, a (310) reflex is clearly visible, which means an incomplete transition (Fig. 4).
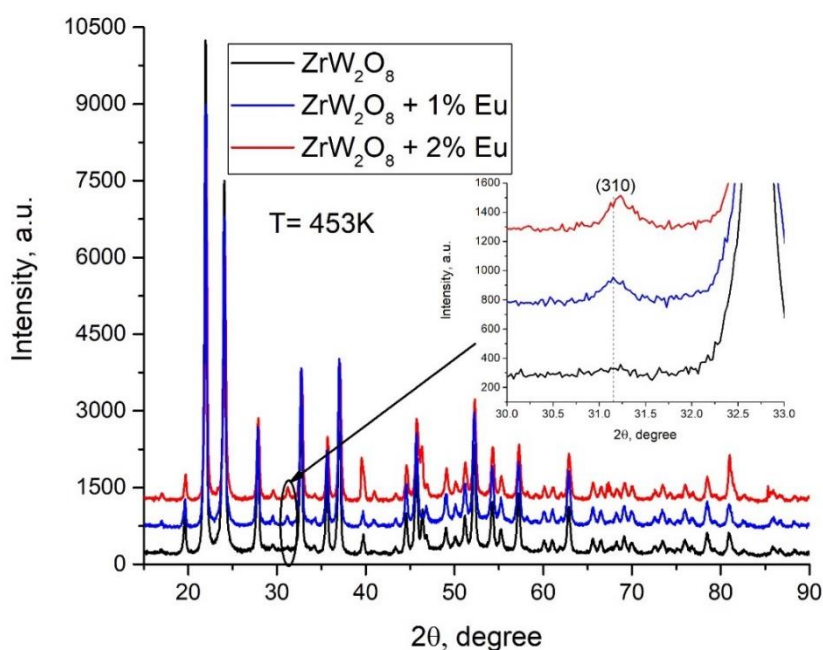

Figure 4. Effect of Eu^{3+} on the phase transition temperature: X-ray patterns of ZrW_2O_8 pure and modified with 1 and 2 mol % Eu^{3+} at 453 K, $Zr_{1-x}Eu_xW_2O_{8-x/2}$; x=0.01, 0.02

The high-temperature X-ray diffraction patterns of the 1 and 3% Tb^{3+} modified samples show that the modifying agent has no effect on the phase transition temperature (Fig. 5). This is established by tracing the (310) reflex, which at 180 °C (453 K) is absent in the unmodified sample, i.e., a proof of a complete phase transition, as the Tb^{3+} modified samples are practically analogous to pure ZrW_2O_8.

The different influence of Eu^{3+} and Tb^{3+} on the phase transition temperature of the modified samples could not be due to the difference in the ionic radii, as it is insignificant: 94.7 and 92.3 pm, respectively. A possible partial conversion of Tb^{3+} to Tb^{4+} under the conditions of preparation of the modified samples can be assumed. The radius of Tb^{4+}, 76 pm, is significantly smaller than the radius of Tb^{3+}, 92.3 pm, but nevertheless closer to the radius of Zr^{4+}, 72 pm. This means a weaker influence or absence of influence on the phase transition

10

temperature upon partial substitution of Zr^{4+} with the close in size Tb^{4+}. (The values of the ionic radii are given for the octahedral coordination of the ion, coordination number 6, according to [3]). The calcination temperature of the samples, 600 °C, was not sufficient to convert Tb^{3+} to Tb^{4+}, but a similar partial conversion was observed in the hydrothermal synthesis of metal-organic frameworks by heating at 140 °C for 72 h. [4].
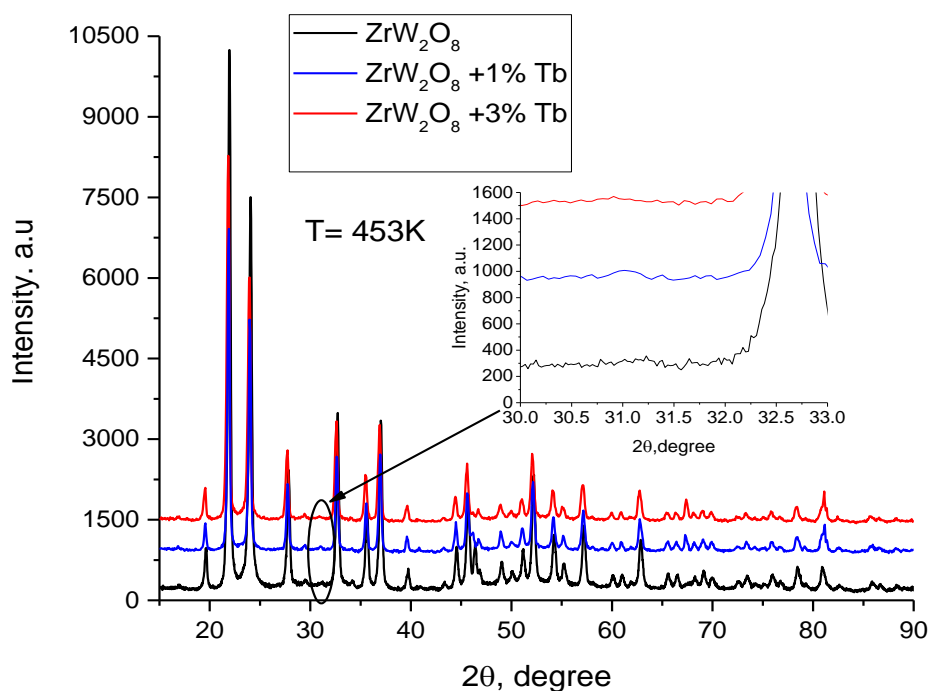

Figure 5. Influence of Tb^{3+} on the phase transition temperature: X-ray patterns of ZrW_2O_8, pure and modified with 1 and 3 mol % Tb3+, at 453 K, $Zr_{1-x}Tb_xW_2O_{8-x/2}$; x=0,01, 0,03

Phase transition with complete inversion α-ZrW_2O_8 ⇌ β-ZrW_2O_8 after cooling back to 25 °C is shown in Figure 6. The difference in the structure of the α-ZrW_2O_8 and β-ZrW_2O_8 phases is presented. The low-temperature α-ZrW_2O_8 phase is built of ZrO_6 octahedra and WO_4 tetrahedra connected by oxygen atoms. Each WO_4 tetrahedron shares three oxygens with neighboring octahedra. In the high-temperature β-ZrW_2O_8 phase, two crystallographically distinct WO_4 tetrahedra share three bonded O atoms. The transition α-ZrW_2O_8→β-ZrW_2O_8 phase called "array - disarray" or "ordered - disordered" phase transition depends on the orientation of the WO_4 tetrahedra.
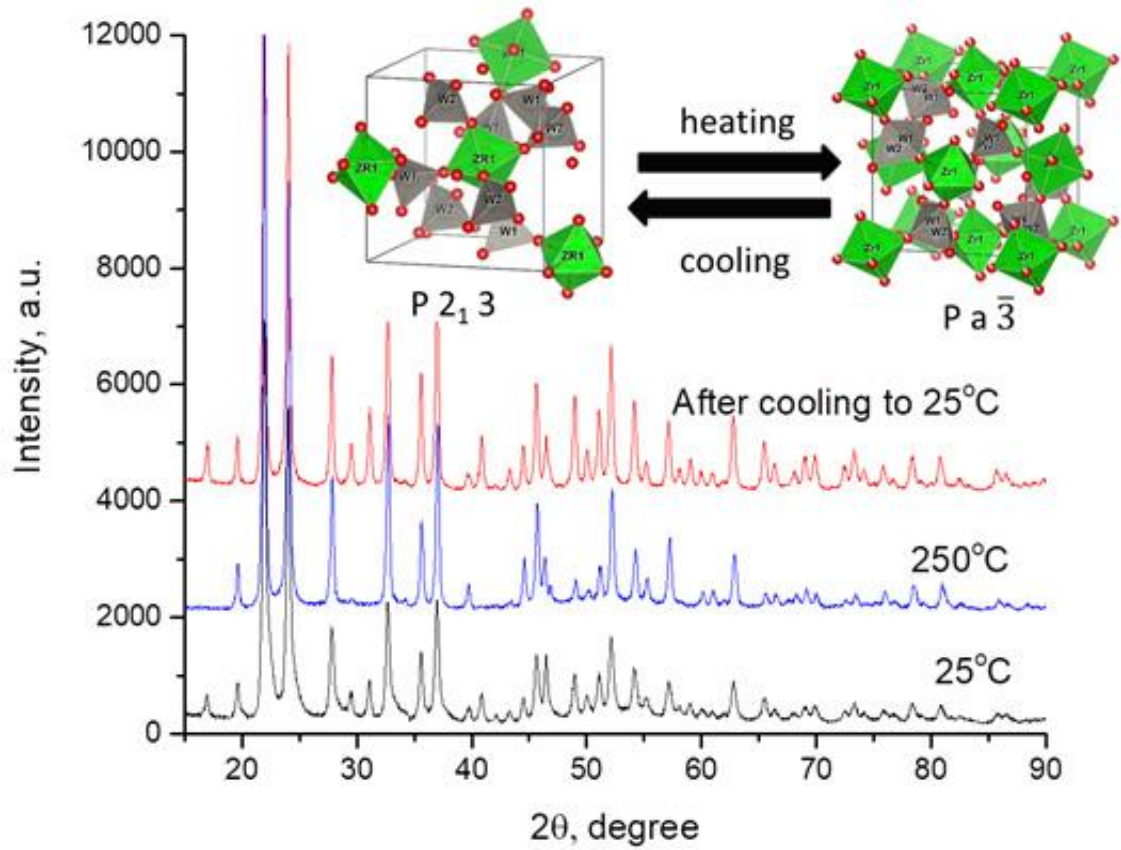
Figure 6. Reversibility of the phase transition α-ZrW$_2$O$_8$ ⇌ β-ZrW$_2$O$_8$; X-ray patterns for ZrW$_2$O$_8$ at 25 and 250 °C and after cooling back to 25 °C [P1, D1, D2]

II.3. Degree of WO$_4$-tetrahedra ordering as a function of temperature

The parameter η'_T has been proposed to estimate the degree of order of WO$_4$ tetrahedra as a function of temperature [1]. It is calculated by the intensity of reflex (310) (disappearing above the phase transition temperature) versus (210) (does not change) using the formula:

$$\eta'_T = \sqrt{\frac{\left[\left(\dfrac{I_{310}}{I_{210}}\right)\right]_T}{\left[\left(\dfrac{I_{310}}{I_{210}}\right)_{ZrW_2O_8}\right]_{298K}}}$$
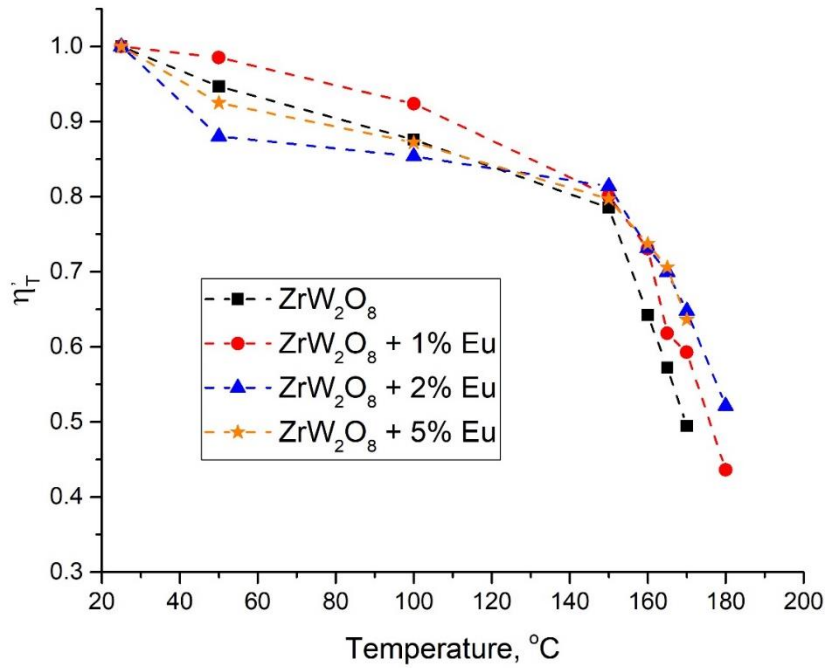
12

Figure 7. Effect of temperature and the modifying agent Eu^{3+}
on the disorder of WO_4 - tetrahedra for $Zr_{1-x}Eu_xW_2O_{8-x/2}$; x= 0.01, 0.02, 0.05

Increase in the content of the modifying Eu^{3+} shifts the approach of η'_T to zero (that is, to complete disorder) to higher temperatures (Fig. 7). The temperature at which the parameter η'_T approaches and becomes equal to zero, $\eta'_T = 0$, is known as the phase transition temperature and can be determined by extrapolating η'_T to zero [1]. Thus, values of 171, 183, 187, 188 °C (444, 456, 460, 461 K) were obtained for pure ZrW_2O_8 and for ZrW_2O_8 modified with 1%, 2% and 5% Eu, respectively.

The temperature dependence of the phase transition upon increasing the content of the modifying Eu^{3+} ion witnessed by us is different from the results published in the literature [1]. A possible reason for the discord is the incomplete crystallization of the samples. Small average crystallite size was observed, as can be seen from the data in Table 1. The crystallites continued to grow during the measurements in the range 25–250 °C, from 24 to 28 nm for the sample with 1 mol % Eu^{3+} and from 20 to 29 nm, respectively, for the sample with 2 mol % Eu^{3+}. This secondary recrystallization probably leads to a further rearrangement of the WO_4 tetrahedra – as a result, a shift of the curve to a higher temperature is registered.

II.4. Coefficients of thermal expansion (CTE)

The coefficients of thermal expansion (CTE) calculated for the interval 25–100 °C (α-ZrW_2O_8 phase) and 200–250 °C (β-ZrW_2O_8 phase) are presented in Table 1.

The calculations were made according to the classical formula for linear thermal expansion: $\alpha = \dfrac{(a_{T2} - a_{T1})}{a_{T1} \cdot \Delta T}$, where α is the coefficient of linear expansion, a_{T1} and a a_{T2} are the unit cell parameters at low and high temperature, ΔT is the temperature difference. In the discussions and comparisons of CTEs for the various modifications, we mean the absolute, not the algebraic, value of CTE.

Table 1. Influence of Ln^{3+}, Ln = Eu, Tb

		ZrW_2O_8	ZrW_2O_8 1 mol % Eu	ZrW_2O_8 2 mol % Eu	ZrW_2O_8 1 mol % Tb	ZrW_2O_8 3 mol %Tb
Size of crystallites, nm	25 °C	26	24	20	28	30
	250 °C	31	28	29	29	31
CTE, × $10^{-6} K^{-1}$	25 °C	-10,8	-7,4	-9,3	-6,5	-7,3
	250 °C	-5,4	-3,6	-2,8	-2,9	- 4,5
Unit cell parameter, Å	25 °C	9,15700(9)	9,15499(2)	9,15281(8)	9,15154(24)	9,14928(46)
	100 °C	9,14956(5)	9,14997(7)	9,14639(6)	9,14557(33)	9,14430(45)
	200 °C	9,13174(3)	9,13172(11)	9,13322(4)	9,13274(41)	9,13291(39)
	250 °C	9,12925(10)	9,13009(7)	9,13192(12)	9,13140(40)	9,13087(39)

The results show *(i)* Values obtained for the coefficient of the negative thermal expansion, NTE, for α- and β - ZrW_2O_8 are higher than the literature data ($-10,2 \times 10^{-6}$ K^{-1}, 30 - 120 °C [5]) (-9,1 $\times 10^{-6}$ K^{-1} / -5,0 $\times 10^{-6}$ K^{-1} [6] , but at different procedure for synthesis *(ii)* The absolute value for the NTE coefficient for both modiffications of $Zr_{1-x}Ln_xW_2O_{8-x/2}$ decreases both in comparison to ZrW_2O_8, as well as in direction Eu - Tb at x = 0.01 i.e. the modification with Ln^{3+} limits the negative expanssion (shrinking) of the crystal cell quite likely because of the partial substitution of Zr^{4+} with Eu^{3+}/Tb^{3+}.

II.5. Unit cell parameter variation

The variation of the unit cell parameter with the temperature and the Eu^{3+} and Tb^{3+} content is presented in Fig. 8 and 9.
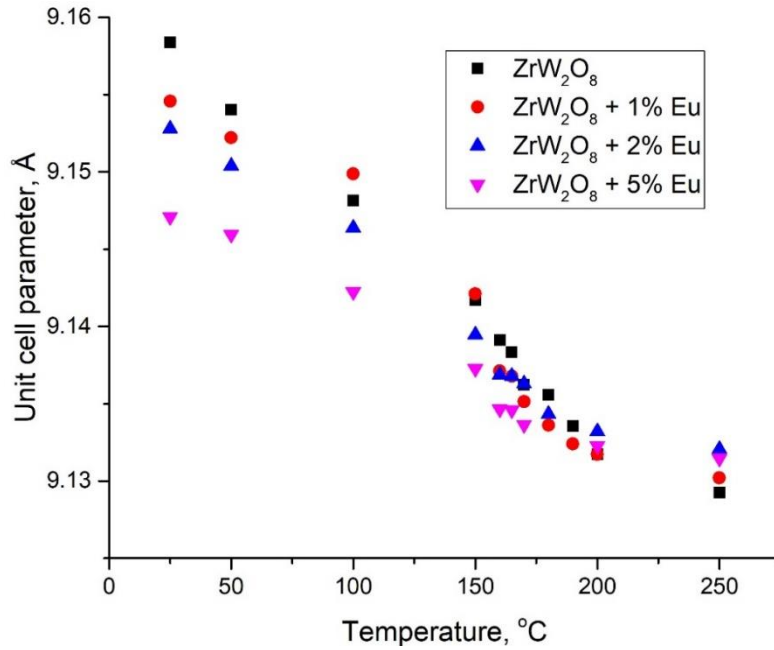

Figure 8. Variation of the unit cell parameter with increase of temperature and Eu^{3+} content for $Zr_{1-x}Eu_xW_2O_{8-x/2}$; x= 0,01, 0,02, 0,05

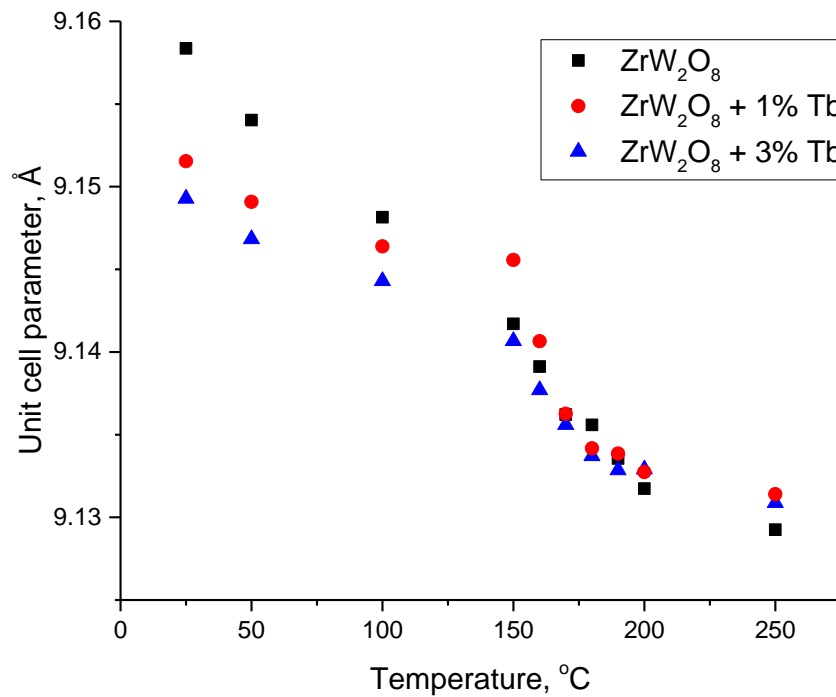**Figure 9.** Variation of the unit cell parameter with increase of temperature and Tb^{3+} content for $Zr_{1-x}Tb_xW_2O_{8-x/2}$; x = 0,01, 0,03

Modification with Eu^{3+} and Tb^{3+} causes a decrease in the unit cell parameter (Table 1). This can be explained by a partial replacement of Zr^{4+} by Eu^{3+}/Tb^{3+}, resulting in a solid solution of the type $Zr_{1-x}Ln_xW_2O_{8-x/2}$. The unit cell parameter also decreases as a function of temperature, which is to be expected due to the negative coefficient of thermal expansion, NTE of ZrW_2O_8. The minor increase of the unit cell parameter in the modified samples compared to the pure ZrW_2O_8 observed at 200-250 °C, is related to the smaller absolute CTE value.

II.6. Energy gap band

Tungstates are semiconductors with a bandgap energy in the range 2.1–4.8 eV for compounds with formula AWO_4 [7, 8]. The band gap for $AgLn(WO_4)_2$ type double tungstates shows values between 3.48 and 4.00 eV for all Ln^{3+}, including Y^{3+}, and is indicative of an allowed indirect transition [9]. The value for ZrW_2O_8 for an indirect transition is 2.84 eV [10]. The band gap energy for the obtained samples was calculated on the basis of UV/Vis spectra, which are presented in Fig. 10, assuming that a direct type of transition takes place. For unmodified ZrW_2O_8, a value of 3.95 eV was obtained, while for the samples modified with 1 and 2 mol % Eu^{3+}, the band gap energy was higher, essentially the same, 4.33 eV. For the sample with 5 mol % Eu^{3+}, the band gap energy grows to 4.45 eV, i.e., values increase with the content of modifying Eu^{3+}, with the highest value obtained at the highest content.
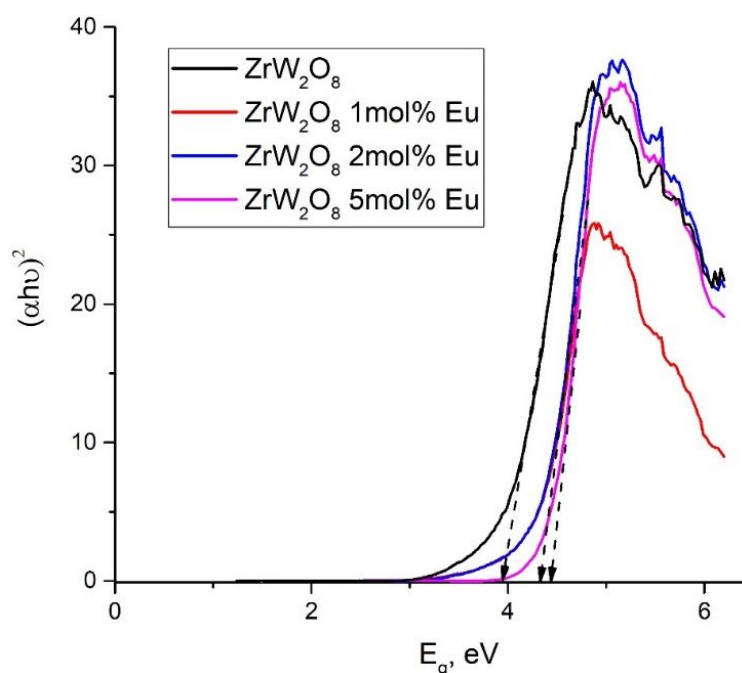

Figure 10. Band gap energy values based on UV/Vis spectra for
$Zr_{1-x}Eu_xW_2O_{8-x/2}$; x= 0,01, 0,02, 0,05

The position of the Eu^{3+} modifier in the crystal lattice was not established. Accounting for the change in the crystal lattice parameter, its position can be assumed both in the crystal lattice and on the surface of the sample out of general considerations. A possible reason for the effect of Eu^{3+} on the band gap energy expansion is the reduced average crystallite size. It is known that the presence of Ln^{3+} can suppress the crystallite growth rate [11]. Pure ZrW_2O_8 has an average crystallite size of 26 nm (Table 1), and the sample modified with 5 mol % Eu^{3+} – 19 nm. The smaller crystallite size suggests quantum effects that widen the band gap [12].

II.7. Conclusions

1. Homogenious crystal samples of $Zr_{1-x}Ln_xW_2O_{8-x/2}$, Ln = Eu^{3+} (x=0,01, 0,02, 0,05) and Tb^{3+} (x=0,01, 0,03) are obtained.

2. The phase transition α-$ZrW_2O_8 \rightarrow \beta$-$ZrW_2O_8$ by the change in the (110) and (310) in the diffractograms with the temperature are confirmed.

3. Different influence of Eu^{3+} and Tb^{3+} on the temperature of the phase transition in the solid solutions is observed, namely increasing in Eu^{3+} - and without change in Tb^{3+} - containing samples. It can be suggested that partially transformation of Tb^{3+} to Tb^{4+} during the synthesis, followed by partial substitution of Zr^{4+} with the closer in size Tb^{4+} does not cause any change in the temperature of the phase transformation.

4. Values for the temperature of the phase transformation for ZrW_2O_8 and $Zr_{1-x}Eu_xW_2O_{8-x/2}$, Ln = Eu^{3+} (x=0.01, 0,02, 0,05), higher than the literature data are probably due to secondary recrystallization causing rearrangement of WO_4 tetrahedra.

5. The presence of Eu^{3+}/Tb^{3+} in the ZrW_2O_8 crystal structure is leading to smaller unit cell parameters, lower absolute value for NTE for low- and high- temperature modifications.

6. An expansion of the forbidden zone with an increase in the content of the modifier was found in the case of Eu^{3+}.

III. Solid solutions $Hf_{1-x}Ln_xW_2O_8$ (Ln = Eu, Tm, Lu) [P2, D4]

III.1. Characterization of α-HfW_2O_8 и β-HfW_2O_8 by X-ray phase analysis

To evaluate the structure of the obtained solid solutions, the structures of α-HfW_2O_8 and β-HfW_2O_8 are needed. The available ICSD database does not contain ".cif files" of α-HfW_2O_8 or β-HfW_2O_8, so to represent the structure of α-HfW_2O_8 we used the .cif file for the α-ZrW_2O_8 modification (ICSD PDF #50-1868), which is isostructural to α-HfW_2O_8. As for β-HfW_2O_8, the

.cif file of the structure $ZrW_{0.977}Mo_{1.023}O_8$ (ICSD PDF #01-070-6112), which is isostructural to β-HfW_2O_8 [13], was used. The diffractograms of the low-temperature α-HfW_2O_8 and the high-temperature β-HfW_2O_8 modifications synthesized by the hydrothermal method, along with the mentioned ICSD data, are shown in Fig. 11. The two reflexes, reflexes (110) and (310), most sensitive to the change, are indicated as present/absent in both modifications.

Table 2. Initial structural parameters

Atom	x	y	z	U_{iso}	Population
Hf1	0.0000	0.0000	0.0000	0.0184	1-x
Ln1	0.0000	0.0000	0.0000	0.0184	x (0.01 или 0.05)
W1	0.3381	0.3381	0.3381	0.0238	0.5
W2	0.6034	0.6034	0.6034	0.0238	0.5
O1	0.2090	0.4326	0.4440	0.0333	1
O3	0.5	0.5	0.5	0.0438	1
O4	0.2326	0.2326	0.2326	0.0476	1

To solve the structure of β-HfW_2O_8 (and the corresponding solid solutions), the initial structural parameters proposed by Kumeswari and co-authors in solving the structure of $ZrW_{0.977}Mo_{1.023}O_8$ [13] were used. The initial structural parameters for our sampes after modification are presented in Table 2.

The following constraints were used when solving the structure: the sum of the Hf-position populations is equal to the total sum of ions introduced during synthesis. The position of O3 was not a free variable due to its location in the crystallographic center of symmetry.
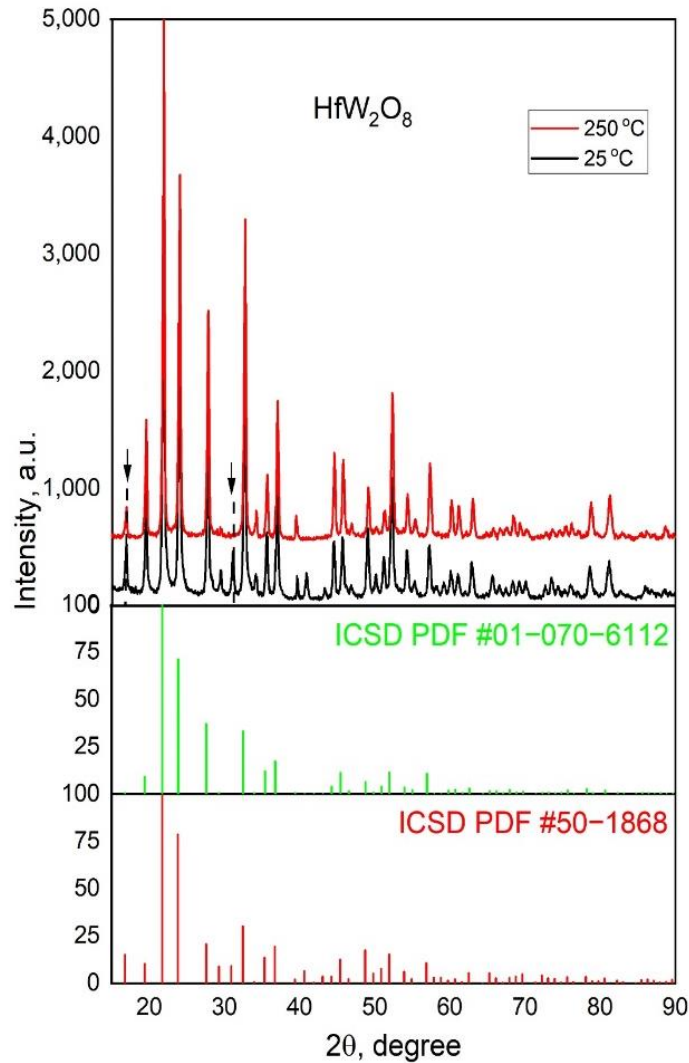
Figure 11. Comparison of the X-ray patterns of α-HfW$_2$O$_8$ and β-HfW$_2$O$_8$ (top), versus ICSD database for α-ZrW$_2$O$_8$ (bottom), and ZrW$_{0.977}$Mo$_{1.023}$O$_8$ (middle)

III.2. Solubility of lanthanide ions in Hf$_{1-x}$Ln$_x$W$_2$O$_{8-x/2}$

By introducing Ln^{3+} ions into the HfW$_2$O$_8$ structure, free oxygen vacancies are generated, and the general formula of the obtained solid solutions can be given by the formula Hf$_{1-x}$Ln$_x$W$_2$O$_{8-x/2}$. It is generally accepted that the obtained in this way oxygen vacancies are deemed intrinsic but are not precisely measured. It is important to note that during the Rietveld-analysis modeling, the occupancy of all O atoms was varied, but due to the very low concentration of these defects, no large deviations were detected. X-ray patterns of samples Hf$_{1-x}$Eu$_x$W$_2$O$_{8-x/2}$, $0{,}01 \leq x \leq 0{,}15$ were recorded at 25 °C and show crystal structure and reflections characteristic for HfW$_2$O$_8$ (Fig. 12).

The reflections observed in the $Hf_{1-x}Eu_xW_2O_{8-x/2}$ samples with x = 0.09 to x = 0.15 indicate the formation of a secondary WO_3 phase. Based on this, it can be said that the obtained samples of $Hf_{1-x}Ln_xW_2O_{8-x/2}$ are phase homogeneous up to x = 0.07 (7 mol %), as evidenced by the powder X-ray patterns of $Hf_{1-x}Eu_xW_2O_{8-x/2}$. Given this, we focused further investigations on the $Hf_{1-x}Ln_xW_2O_{8-x/2}$ solid solutions, with x = 0.01 and 0.05. Solid solutions of lutetium-modified hafnium tungstate $Hf_{1-x}Lu_x W_2O_{8-x/2}$ were obtained at x=0.02 and 0.04 by solid-phase synthesis [14].
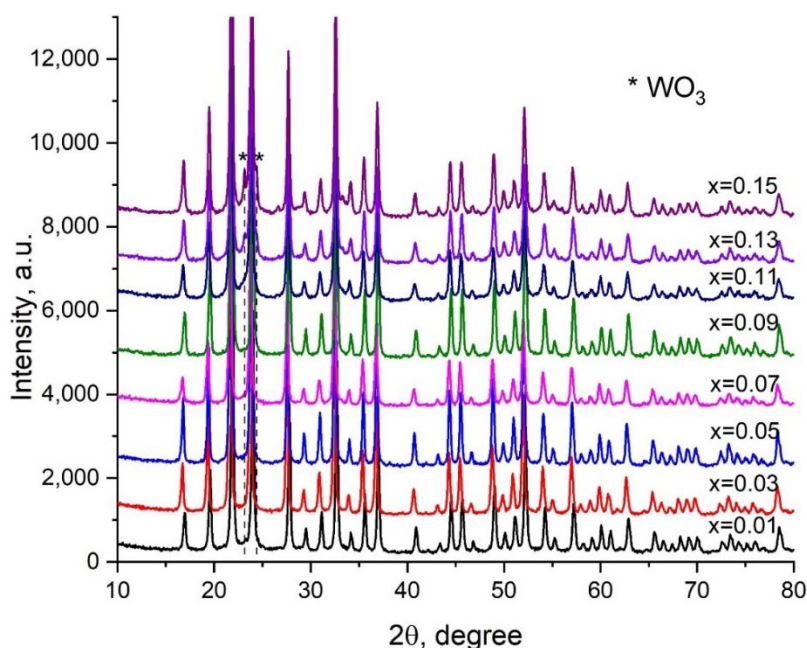

Figure 12. X-ray patterns of solid solutions of the type $Hf_{1-x}Eu_xW_2O_{8-x/2}$, 0,01 ≤ x ≤ 0,15, taken at 25 °C

III.3. Characterization by Raman and IR spectroscopy

Raman spectroscopy is an effective and sensitive method for tracking changes in the position and bonds between W and O atoms in the crystal lattice [15]. Raman spectra were taken for pure α-HfW_2O_8 and $Hf_{1-x}Ln_xW_2O_{8-x/2}$ solid solutions, at x = 0.01 and 0.05. The structure of α-HfW_2O_8 is considered as a network of WO_4 octahedra and tetrahedra sharing common vertices, and the Raman vibrations of tungstates can be lattice, translational, vibrational and internal vibrations of WO_4 in the range $100 - 1100$ cm^{-1} [16, 17]. In the Raman spectrum of pure α-HfW_2O_8, bands in the range 400–100 and 1040–700 cm^{-1} are observed (Fig. 13, a, b).

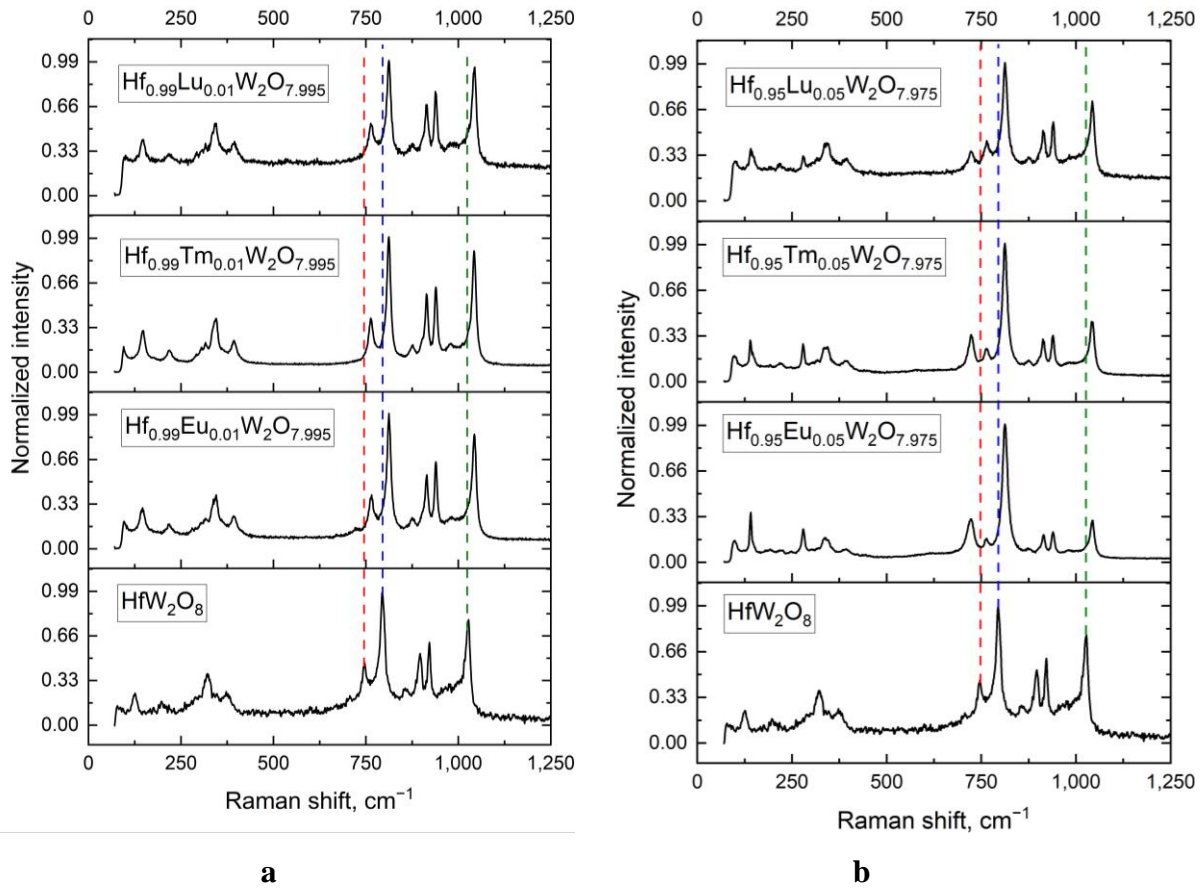**Figure 13.** Raman spectra of HW_2O_8 and $Hf_{1-x}Ln_xW_2O_{8-x/2}$, (a) x = 0.01 and (b) x = 0.05 The colored dashed lines indicate shifts of the corresponding bands relative to those in pure tungstate as a result of the modification

Based on literature data [18], the bands at 1026, 999, 921, 896 and 859 cm^{-1} were assigned to the symmetric valence vibrations of WO_4; those at 796 and 746 cm^{-1} – to the asymmetric valence vibrations of WO_4 (modi v_{as}); at 373 cm^{-1} – to an asymmetric deformation oscillation; at 346, 323, and 297 cm^{-1} – to symmetric deformation vibrations. The bands at 199 and 125 cm^{-1} are considered to originate from lattice vibrations (Fig. 13, a, b).

In the Raman spectra of the obtained $Hf_{1-x}Ln_xW_2O_{8-x/2}$ solid solutions, a shift of the bands to higher frequencies is observed (Fig. 13, a, b). This shift affects the bands assigned to vibrations of the W-O-W bonds (WO_4) of HfW_2O_8, namely at 796 cm^{-1} (most intense) and 746 cm^{-1} (less intense). The two bands are shifted by about 18 cm^{-1} to 812–813 and 764–765 cm^{-1}, respectively, in the $Hf_{1-x}Ln_xW_2O_{8-x/2}$ solid solutions for x = 0.01 and x = 0.05 (Figure 13, a, b). Furthermore, a new band at 721, 723, 724 cm^{-1} was found in the spectra of $Hf_{0.95}Ln_{0.05}W_2O_{7.975}$, for Eu, Tm and Lu, respectively. At the same time, the shift of the band at 1026 cm^{-1} for pure

α-HfW_2O_8 by about 18 cm^{-1} to 1043 cm^{-1} in the solid solutions $Hf_{0.99}Ln_{0.01}W_2O_{7.995}$ and $Hf_{0.95}Ln_{0.05}W_2O_{7.975}$ is a clear evidence of the influence of Ln^{3+} on the crystal structure.

The influence of lanthanide ions on the Raman spectra of the modified samples $Hf_{1-x}Ln_xW_2O_{8-x/2}$ can be considered as a result of partial replacement of Hf^{4+} by Ln^{3+} in the HfO_6 octahedra. This affects the length of the Hf-O-W bond, which affects the arrangement and rotation of the WO_4 tetrahedra, and thereof also the valence vibrations of the W-O-W bonds.

We assume that the influence is determined by both the ionic radius of the lanthanide ion and the atomic mass. The atomic mass affects through the effective mass m according to the formula for the oscillation frequency $\nu = \frac{1}{2\pi}\sqrt{\frac{k}{m}}$. The formula gives the frequency of oscillations for a diatomic molecule, where k is the force constant, m effective mass ($m_1 \times m_2/m_1 + m_2$), m_1 и m_2 are the atomic masses of the atoms in the diatomic molecule under consideration [19]. Since only Hf is partially substituted in Hf-O-W, we reduce the consideration to a diatomic molecule and consider the atomic masses of hafnium (or the lanthanide ion replacing it) and of the oxygen atom.

The partial substitution of Hf^{4+} with the having bigger size, but smaller atomic mass, Eu^{3+} (effective mass m in the formula is 14,48/14,68 for Hf), is causing the schange in the of the intensity of the band at 1043 cm^{-1} in comparison with Tm^{3+} and Lu^{3+} in$Hf_{0.95}Ln_{0.05}W_2O_{7.975}$. Considering the intensity of the band at 1043 cm^{-1}, a similarity with the Raman spectrum of HfW_2O_8 and $Hf_{0.95}Lu_{0.05}W_2O_{7.975}$ is observed, where Lu^{3+} is with the smallest radius of of the investigated, closest to Hf^{4+}, and with a atomic mass , closest to the atomic mass of Hf^{4+} (the effective mass m in theformula for the frequency 14,66 за Lu /14,68 за Hf) (Fig. 13, b).

In addition, the samples were also characterized by infrared spectroscopy; spectra were taken in the range of 4000–400 cm^{-1} with bands indicating the presence of moisture. In the informative range of 1100–400 cm^{-1}, the absorption bands at 941, 917, 882, 832, 809, 777, and 761 cm^{-1} are marked with dashed lines (Fig. 14).
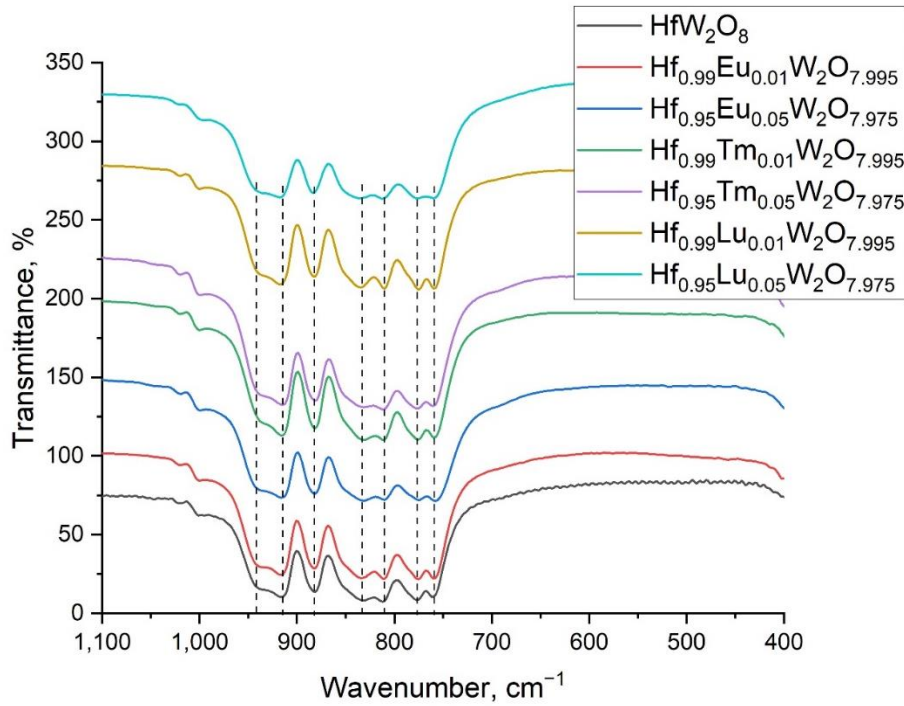
Figure 14. FT–IR spectra of the samples in the range 1100–400 cm^{-1}

The bands are attributed to the symmetric (941, 917, 882 and 832 cm^{-1}) and asymmetric (809, 777 and 761 cm^{-1}) valence vibrations of W-O-W in the WO_4-tetrahedra [18]. Asymmetric and symmetric defformation vibrations, as well as lattice oscillations, were observed below 400 cm^{-1}, but they were not recorded with the FT-IR apparatus used. The influence of Ln^{3+} is visible in the spectrum of $Hf_{0.95}Lu_{0.05}W_2O_{7.975}$ expressed in the broadening of the band at 761 cm^{-1}, which, although weak, is also noticeable in the spectra of other $Hf_{0.95}Ln_{0.05}W_2O_{7.975}$.

III.4. Morphology of samples characterized by electron microscopy (SEM and TEM)

By SEM, acicular crystals were observed both in HfW_2O_8 (Figure 15, a) and in the solid solutions $Hf_{0.99}Eu_{0.01}W_2O_{7.995}$ and $Hf_{0.95}Eu_{0.05}W_2O_{7.975}$ (Figure 15, b,c). that is, Ln^{3+} does not influence the morphology.

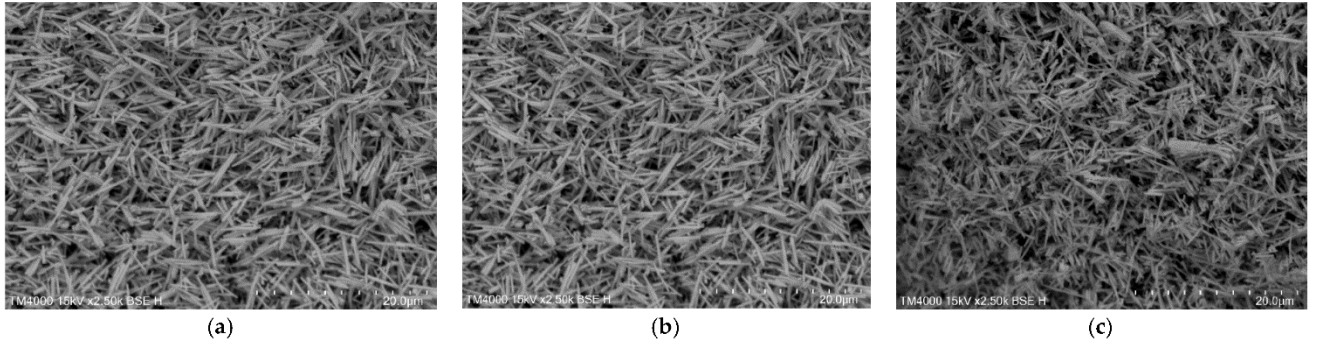**Figure 15.** SEM images of (a) HfW_2O_8, (b) $Hf_{0.99}Eu_{0.01}W_2O_{7.995}$ and (c) $Hf_{0.95}Eu_{0.05}W_2O_{7.975}$

Acicular microcrystals analogous to those observed by SEM were also observed by TEM for α-HfW_2O_8 and the resulting solid solutions. The microcrystals are well shaped and of high crystallinity for $Hf_{0.99}Tm_{0.01}W_2O_{7.99}$ (Fig. 16, a). The length of the microcrystals varies in the range of 2 to 5 μm.

The order in the crystal lattice is high with well-defined crystal planes and interplanar distances for the $Hf_{0.99}Lu_{0.01}W_2O_{7.995}$, $Hf_{0.99}Eu_{0.01}W_2O_{7.995}$, and $Hf_{0.95}Eu_{0.05}W_2O_{7.975}$ solid solutions as shown in Fig. 16 b–d.

The crystal plane in the direction corresponding to the highest diffraction peak in the cubic structure of α-HfW_2O_8 is seen. The interplanar distances (220) and (221) of samples $Hf_{0.95}Eu_{0.05}W_2O_{7.975}$ and $Hf_{0.99}Lu_{0.01}W_2O_{7.995}$ show increasing values for $Hf_{0.95}Eu_{0.05}W_2O_{7.975}$, which is a result of the larger ionic radius of Eu^{3+} (94.7 pm Eu^{3+}, 86.1 pm Lu^{3+} [3]).

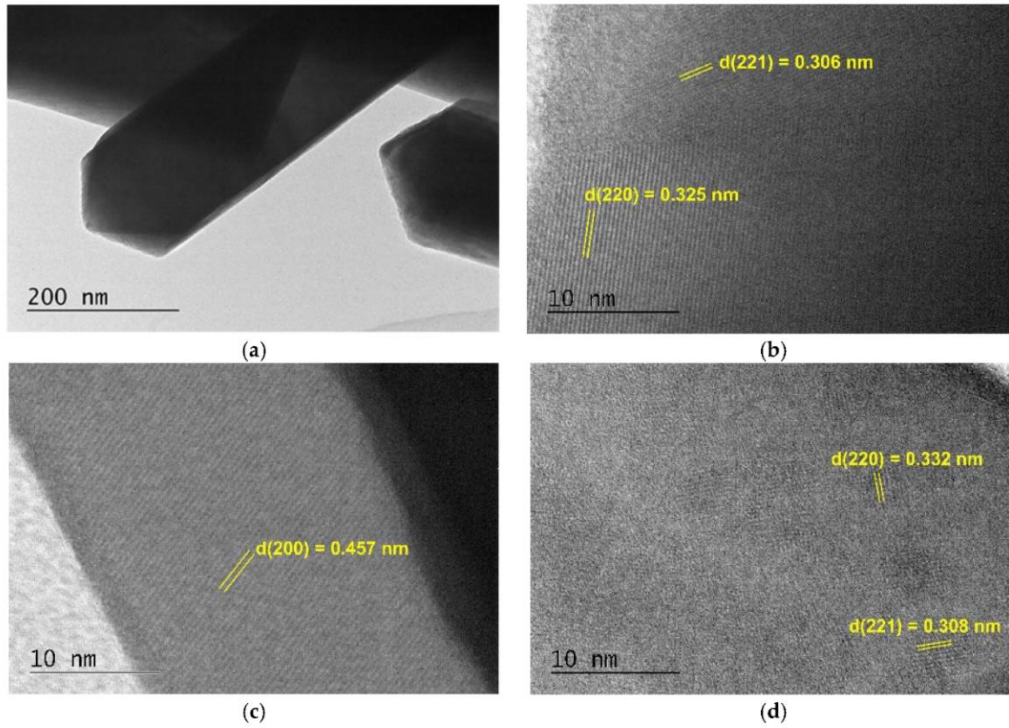**Figure 16.** TEM images: (a) microcrystals of $Hf_{0.99}Tm_{0.01}W_2O_{7.995}$ with well-defined edges, (b) $Hf_{0.99}Lu_{0.01}W_2O_{7.995}$, (c) $Hf_{0.99}Eu_{0.01}W_2O_{7.995}$, and (d) $Hf_{0.95}Eu_{0.05}W_2O_{7.975,}$ showing the internal crystal structure with characteristic interplanar spacing

III.5. Phase transition reversibility, coefficients of thermal expansion for pure HfW_2O_8 and for solid solutions $Hf_{1-x}Ln_xW_2O_{8-x/2}$

III.5.1. Phase transition α-HfW_2O_8 ⇄ β-HfW_2O and its reversibility

X-ray diffractograms of pure HfW_2O_8 were taken in the temperature range 25/250/25 °C, where the reversible transition α-HfW_2O_8⇌ β-HfW_2O_8 is visible (Fig. 17). The reflex at 16.9 2θ only decreases in intensity, while that at 31 2θ decreases and disappears with increase of temperature (indicated by arrows in Fig. 17). While the last two reflexes are typical for α-HfW_2O, their disappearance at 250 °C is a sign of a completed α-$HfW_2O_8 \rightarrow$ β-HfW_2O_8 phase transition. After cooling to 25 °C, these reflexes can be detected again as evidence of the reversibility of the transition (Fig. 17).
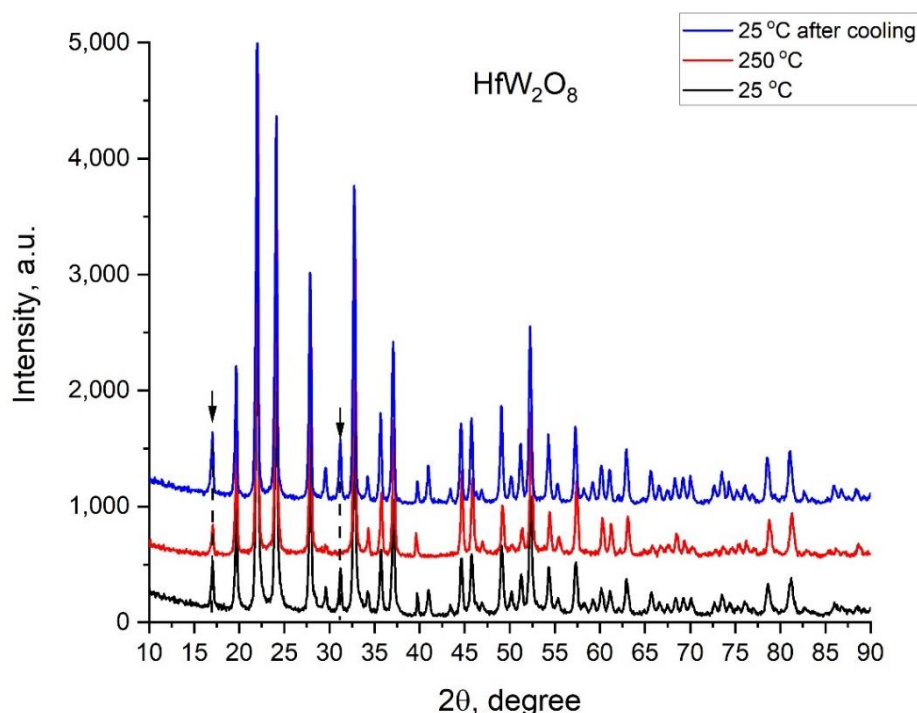
Figure 17. X-ray patterns of pure HfW_2O_8 taken at 25/250/25 °C (from bottom to top) showing the reversibility of the α-$HfW_2O_8 \rightleftharpoons \beta$-$HfW_2O_8$ transition.

The reflexes at 16.9 and 31.1 2θ are indicated

III.5.2. Unit cell parameters and coefficients of thermal expansion

Unit cell parameters for pure HfW_2O_8 and $Hf_{1-x}Ln_xW_2O_{8-x/2}$, x = 0,01 and 0.05, together with thermal expansion coefficients calculated in the interval 25–100 °C (α-HfW_2O_8) and 200–250 °C (β-HfW_2O_8) and 25–250 °C for $Hf_{1-x}Ln_xW_2O_{8-x/2}$, are presented in Table 3.

Considering that HfW_2O_8 has an isotropic coefficient of negative thermal expansion, we used the classical formula for linear expansion (instead of volumetric expansion) [20].

It can be seen that *the cubic unit cell parameter* for pure HfW_2O_8 decreases with *increasing temperature* from 25 to 250 °C, which proves that the cell shrinks and demonstrates the negative coefficient of thermal expansion. The same trend is observed for the unit cell parameter of the $Hf_{0.99}Ln_{0.01}W_2O_{7.995}$ and $Hf_{0.95}Ln_{0.05}W_2O_{7.975}$ solid solutions as the temperature increases (Table 4). *Increasing the Ln^{3+} content* from x = 0.01 to 0.05 has little effect on the unit cell parameter, with a slight decrease observed for the low-temperature α-$Hf_{1-x}Ln_xW_2O_{8-x/2}$ (25 °C) and a slight increase for the high-temperature modification β-$Hf_{1-x}Ln_xW_2O_{8-x/2}$ (250 °C), in both cases within the error range. *Compared to pure* HfW_2O_8, a slight increase in the

26

cubic unit cell parameter of $Hf_{1-x}Ln_xW_2O_{8-x/2}$ is observed, especially for the samples containing Eu^{3+} (Table 3), as a result of the larger ionic radius of Eu^{3+}.

Table 3. Unit cell parameters and CTE values for pure HfW_2O_8 and
$Hf_{1-x}Ln_xW_2O_{8-x/2}$ (x = 0.01 and 0.05)

	T°C	HfW_2O_8	$Hf_{1-x}Eu_xW_2O_{8-x/2}$		$Hf_{1-x}Tm_xW_2O_{8-x/2}$		$Hf_{1-x}Lu_xW_2O_{8-x/2}$	
			x = 0,01	x = 0,05	x = 0,01	x = 0,05	x = 0,01	x = 0,05
Unit cell parameter, Å	25	9.1244(2)	9.1246(3)	9.1245(1)	9.1245(1)	9.1245(1)	9.1244(1)	9.1243(1)
	100	9.1174(1)	9.1179(1)	9.1177(1)	9.1171(1)	9.1170(1)	9.1173(1)	9.1172(1)
	200	9.1055(1)	9.1058(2)	9.1057(1)	9.1050(3)	9.1049(1)	9.1049(1)	9.1048(1)
	250	9.1050(1)	9.1051(1)	9.1053(2)	9.1044(1)	9.1046(1)	9.1044(1)	9.1045(2)
CTE, $\times 10^{-6}$ K^{-1}	25-100	-10.22	-9.79	-9.94	-10.81	-10.96	-10.38	-10.36
	200-250	-1.10	-1.54	-0.87	-1.32	-0.66	-1.10	-0.66
	25-250	-9.45	-9.49	-9.35	-9.79	-9.69	-9.74	-9.64

The *calculated thermal expansion coefficients* are -10.22×10^{-6} and -1.10×10^{-6} K^{-1} for the pure α-HfW_2O_8 and β-HfW_2O_8 phases, respectively (Table 3). These differ from the literature data, -9 and -6×10^{-6} K^{-1} [21], most likely as a result of the different method used for synthesis. The presence of Ln^{3+} in the solid solutions is essential for the α-HfW_2O_8 modification.

The results for the NTE coefficients for HfW_2O_8 differ by those for ZrW_2O_8 (Table 1, II.4., p. 14). At the temperature below the phase transition the values are -10,8 и -10,22 $\times 10^{-6}$ K^{-1}, for ZrW_2O_8 и HfW_2O_8, respectively. Above the phase transition the tendency is kept but with a bigger difference, - 5,4 и -1,10 $\times 10^{-6}$ K^{-1} за ZrW_2O_8 и HfW_2O_8, respectively.

It is logical that increasing the temperature above 250 °C would cause additional shrinkage, but with a decreasing absolute value of the NTE coeficients due to volume shrinkage. The slight shrinkage of hafnium tungstate at the high temperature (250 °C) may be due to:
(i)) difference in the free volume: at 250 °C the volume of the unit cell of ZrW_2O_8 is ~ 761, while for HfW_2O_8 is 755 Å^3; *(ii)* difference in the bond length: 2,0718 for Zr-O, and 2,0660 Å for Hf-O, respectively (our crystallographic calculations). It can be expected that in M-O-M transverse vibrations the shorter Hf-O bond is more inert, the distance between the metal atoms in Hf-O-W is less affected and as a result a weaker rotation of the tetrahedron in the hafnium tungstate structure.

(iii) difference in the atomic mass: The vibrations of the atoms in the lattice are affected by the atomic mass. For a diatomic molecule, the frequency of oscillations is given by the formula: $\nu = \frac{1}{2\pi}\sqrt{\frac{k}{m}}$ (higher frequence for Zr-O, lower for Hf-O). The oscillation amplitude in Zr-O-W will be smaller, the bond will shorten less (i.e. stay longer), in contrast to Hf-O-W, where the oscillation frequency will be smaller, but with a larger amplitude of oscillations. This probably results in a weaker rotation of the tetrahedron in the hafnium tungstate structure.

High-temperature X-ray diffraction patterns of $Hf_{1-x}Ln_xW_2O_{8-x/2}$ (x = 0.01; Ln = Eu, Lu) show that the temperature 140 °C is the critical temperature for the phase transition, that is, the reflex at 31 2θ, typical of α-HfW_2O_8 disappears, which is an indication of complete conversion (Fig. 18 a, b).
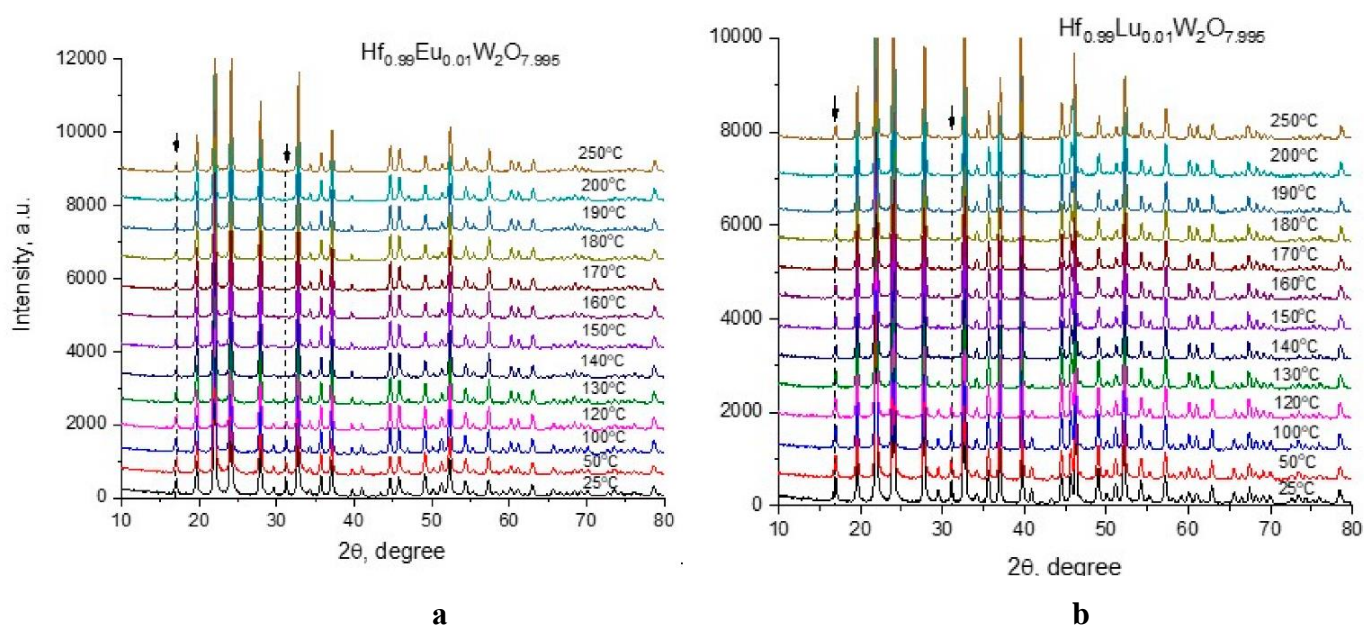

Figure 18. X-ray patterns taken at high temperature for $Hf_{1-x}Ln_xW_2O_{8-x/2}$, x = 0.01; Ln: (a) Eu, (b) Lu; 140 °C is the critical phase transition temperature

III.5.3. Phase transition from order to disorder in $Hf_{1-x}Ln_xW_2O_{8-x/2}$ (x = 0.01; 0.05) and the role of Ln^{3+}

In the structure of the low-temperature α-HfW_2O_8 and the high-temperature β-HfW_2O_8 modifications, the HfO_6-octahedra are connected to the WO_4-tetrahedra by sharing common oxygen atoms (vertices). In the α-HfW_2O_8-modification, each WO_4 tetrahedron shares three of its oxygen atoms with neighboring octahedra, while in the high-temperature β-HfW_2O_8 modification, two WO_4 share three O atoms. The crystal structures of the low-temperature α-$Hf_{1-x}Ln_xW_2O_{8-x/2}$ and

the high-temperature β-$Hf_{1-x}Ln_xW_2O_{8-x/2}$ modification are shown in Fig. 19, where the half-filled WO_4 tetrahedron in β-$Hf_{1-x}Ln_xW_2O_{8-x/2}$ is shown in darker color (grey).
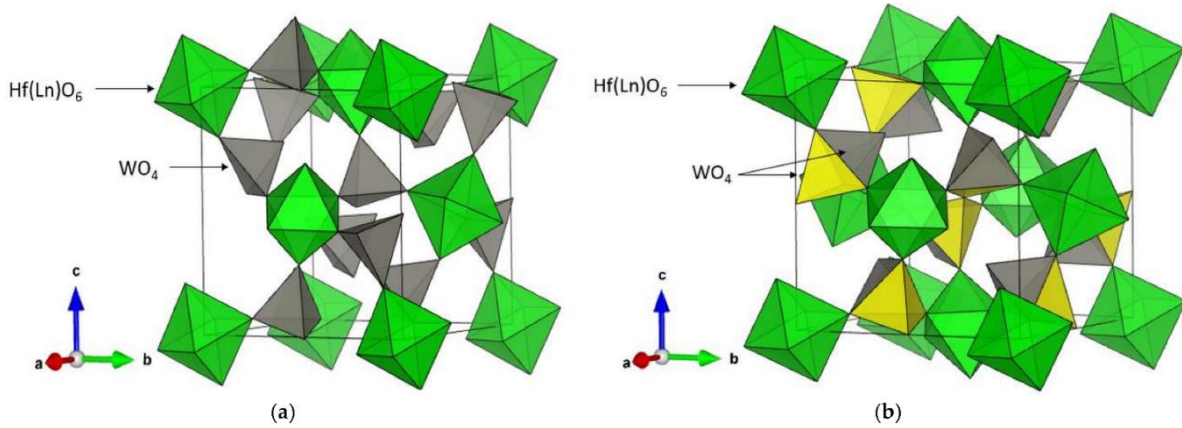

Figure 19. Crystal structures of (a) α-$Hf_{1-x}Ln_xW_2O_{8-x/2}$ and (b) β-$Hf_{1-x}Ln_xW_2O_{8-x/2}$. The yellow and gray tetrahedra in β-$Hf_{1-x}Ln_xW_2O_{8-x/2}$ represent the half-filled WO_4

The orientations of the WO_4-tetrahedra determine the transition α-$HfW_2O_8 \rightarrow \beta$-$HfW_2O_8$, which is a phase transition from order to disorder [22]. The degree of order of the WO_4-tetrahedra is directly dependent on the temperature and can be estimated by the parameter η'_T [1].

$$\eta'_T = \sqrt{\frac{\left[\left(\dfrac{I_{310}}{I_{210}}\right)\right]_T}{\left[\left(\dfrac{I_{310}}{I_{210}}\right)_{HfW_2O_8}\right]_{298K}}}$$

As can be seen in Fig. 20, the relative parameter at room temperature significantly decreases when Eu^{3+} is introduced into the system, resulting in a higher degree of rotation of the WO_4 tetrahedra in $Hf_{0.99}Eu_{0.01}W_2O_{7.995}$. The effect of Tm^{3+} and Lu^{3+} in $Hf_{0.99}Ln_{0.01}W_2O_{7.995}$ solid solutions is less pronounced and can be explained by the degree of solubility. The heavier Ln^{3+} is much more soluble in the system, due to the closer ionic radius to that of Hf^{4+} (Lu^{3+} 86.1, Tm^{3+} 88.0, Eu^{3+} 94.7, Hf^{4+} 72.0 pm, at a coordination number of 6 [3]). In the solid solutions $Hf_{0.95}Ln_{0.05}W_2O_{7.975}$, the most soluble among the investigated ions, Lu^{3+}, has the strongest influence on the degree of order of the tetrahedron, probably due to the most significant inclusion in the crystal structure at the higher content, x= 0, 05.
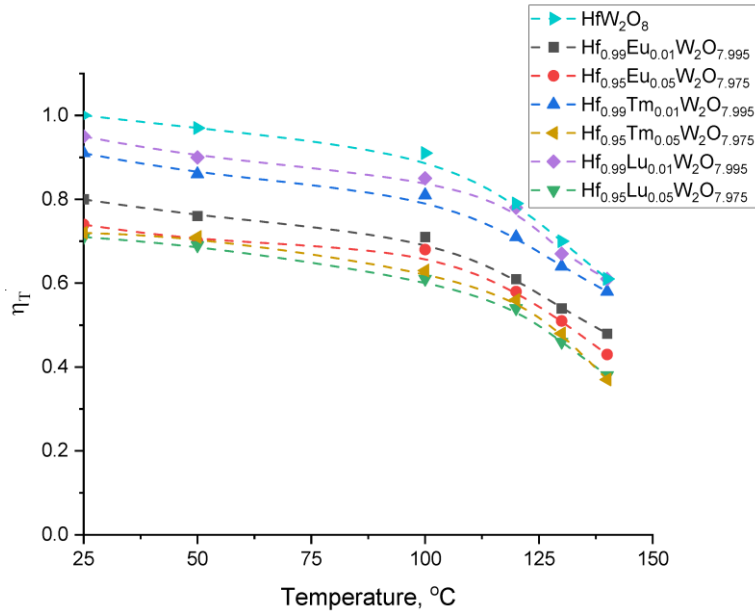
Figure 20. Effect of the temperature and amount of Ln^{3+} in $Hf_{1-x}Ln_xW_2O_{8-x/2}$ solid solutions (x = 0.01 and 0.05) on the disorder of WO_4 tetrahedra

III.6. UV-Vis absorption of solid solutions. Energy gap

The absorbance in the UV-Vis range (200–450 nm) shows a maximum at about 250 nm for all the investigated samples. The observed weak absorption at about 400 nm for $Hf_{1-x}Tm_xW_2O_{8-x/2}$ (x = 0.01 and 0.05) (Fig. 21, a) is not noticeable for the other samples. It is very likely that the bands between 250 and 350 nm exist due to the strong ligand-to-metal charge transfer observed in both slightly distorted monotungstate structures and polytungstates [23].
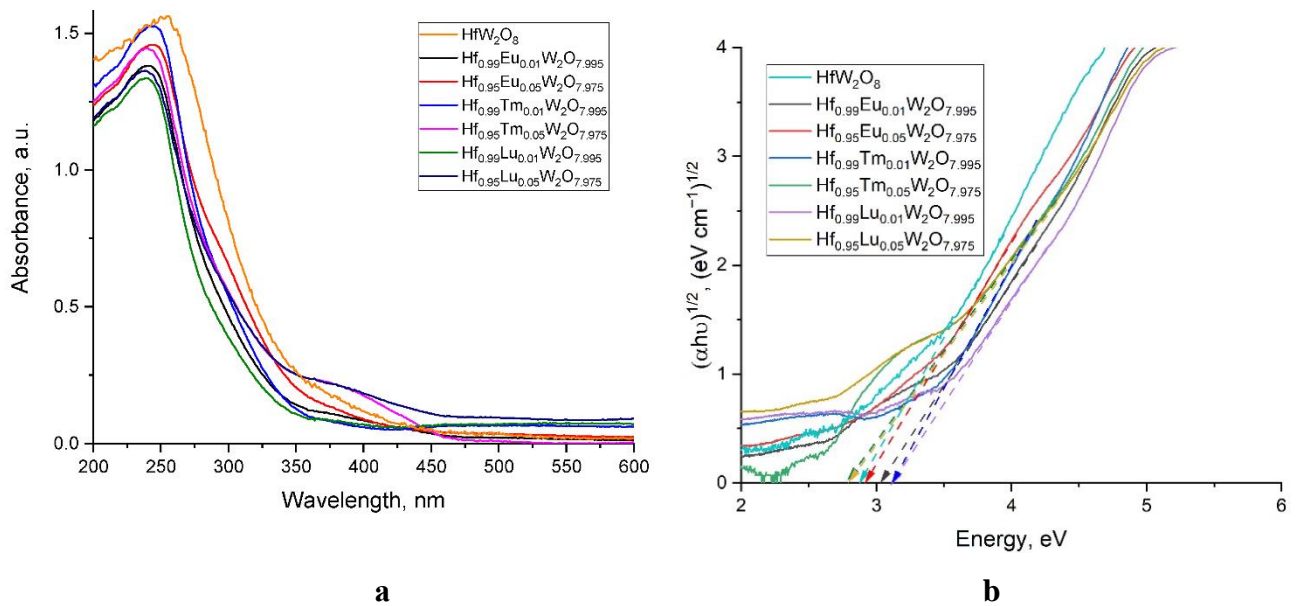

a   b

Figure 21. (a) UV-Vis spectra and (b) band gap energy

The band gap energy calculations were performed based on UV-Vis data (Fig. 21, a, b) and presented in Table 4. The UV-Vis data were analyzed by determining the relationship between the band gap optical width, the coefficient of absorption and the energy (hv) of the incident photon for near-edge optical absorption. The calculations were performed from the measured curves by fits, according to Tauck's formula $\varepsilon hv = A(hv - Eg)^n$ [24], where A is a constant independent on hv, Eg is the gap width, ε is the molar extinction coefficient and n depends on the type of transition. The well-known approach for determination of Eg from the intersection of $(\varepsilon hv)^{1/n}$, versus hv along the x-axis was used, with n being 1/2 and 2 for direct and indirect transitions, respectively.

Table 4. Band gap energy of HfW_2O_8 and the solid solutions, eV

№	Sample	E_g, eV
1	HfW_2O_8	2,87
2	$Hf_{0.99}Eu_{0.01}W_2O_{7,995}$	3,02
3	$Hf_{0.95}Eu_{0.05}W_2O_{7.975}$	2,92
4	$Hf_{0.99}Tm_{0.01}W_2O_{7.995}$	3,10
5	$Hf_{0.95}Tm_{0.05}W_2O_{7.975}$	2,78
6	$Hf_{0.99}Lu_{0.01}W_2O_{7.995}$	3,12
7	$Hf_{0.95}Lu_{0.05}W_2O_{7.975}$	2,78

The band gap energy obtained by Tauck's equation of pure α-HfW_2O_8 is 2.87 eV, and matches well the value observed for pure α-ZrW_2O_8, 2.84 eV for direct transition [9]. The solid solution values for all samples of the type $Hf_{0.99}Ln_{0.01}W_2O_{7.995}$, x = 0.01 increase to 3.02, 3.10, and 3.12 eV, for Ln = Eu^{3+}, Tm^{3+} and Lu^{3+}, respectively. This may be due to the decrease in crystallite size owed to the presence of Lu^{3+} [10]. Interestingly, further incorporation of Ln^{3+} in $Hf_{0.95}Ln_{0.05}W_2O_{7.975}$, x = 0.05, leads to a significant narrowing of the band gap, especially for Tm^{3+} and Lu^{3+} (2.78 eV). This is most likely due to the higher degree of rotation of the WO_4 polyhedra as a result of more significant incorporation of the smaller ions into the HfO_6 octahedra upon substitution of Hf^{4+}. A similar effect, caused by a high-pressure-induced amorphization, was observed by Muthu and co-authors [7].

III.7. Conclusions

1.The structure of the polymorphic modification β-HfW$_2$O$_8$ was solved, which allowed to solve the structure of the high-temperature modifications of the obtained solid solutions Hf$_{1-x}$Ln$_x$W$_2$O$_8$ (Ln = Eu, Tm, Lu).

2. The occurrence of the α-HfW$_2$O$_8$ → β-HfW$_2$O$_8$ phase transition was confirmed by monitoring the change of the (110) and (310) reflections in the X-ray images with increasing temperature.

3. The established differences in the absolute values of NTE coefficients for ZrW$_2$O$_8$ and HfW$_2$O$_8$, greater in the high-temperature modifications, may be due to differences in atomic masses, as well as in the free volume and the bond length.

4. Based on the high-temperature X-ray diffraction patterns of the solid solutions Hf$_{1-x}$Ln$_x$W$_2$O$_{8-x}$/$_2$ (x = 0.01; Ln = Eu, Lu), the phase transition temperature was determined.

5. A difference was found in the influence of lanthanide ions on (i) band gap energy values for Hf$_{1-x}$Ln$_x$W$_2$O$_8$ (Ln = Eu, Tm, Lu); (ii) the coefficients of thermal expansion, where Hf$_{1-x}$Lu$_x$W$_2$O$_8$ (Lu^{3+} with the smallest ionic radius among the studied lanthanides, with an atomic mass closest to hafnium) shows values closest to β-HfW$_2$O$_8$.

IV. SUMMARY AND CONCLUSIONS

1. ZrW$_2$O$_8$ and HfW$_2$O$_8$ were modified by a hydrothermal method and solid solutions M$_{1-x}$Ln$_x$W$_2$O$_8$ (M = Zr, Hf; Ln = Eu, Tb, Tm, Lu) were obtained, for which the influence of the modifying lanthanide ions on *(i)* the parameter of the unit cell, *(ii)* the phase transition temperature, *(iii)* the coefficient of thermal expansion, *(iv)* the band gap energy, *(v)* the valence vibrations of W-O-W in the Raman spectra were established. A relatively low value of the limiting content of the modifying lanthanide ion, x = 0.07, was found, at which a phase-homogeneous solid solution Hf$_{1-x}$Ln$_x$W$_2$O$_8$ (Ln = Eu, Tm, Lu) was obtained.

2. The use of available data on isostructural compounds, as well as literature data on initial structural parameters, allowed by solving the structure of the polymorphic modification β-HfW$_2$O$_8$ to also solve the structure of the high-temperature modifications of the obtained solid solutions.

3. The values obtained for NTE for the low-temperature modifications alfa-ZrW$_2$O$_8$ and alfa-HfW$_2$O$_8$ are very close, while the values for the high-temperature modifications beta-

ZrW_2O_8 and beta-HfW_2O_8 differ significantly, and the low absolute value for beta-HfW_2O_8 also differs significantly from the literature data, which may also be due to the method of synthesis.The observed minor shrinkage in beta-HfW_2O_8 compared to beta-ZrW_2O_8 may result from difference in (i) Zr/Hf atomic mass, (ii) Zr-O/Hf-O bond length, (iii) free volume of the crystal lattice, but the influence of other factors, such as synthesis methods, their reproducibility, especially bearing in mind the established difference between our and literature data, but also between literature data from different sources, is also possible.

4. The studied properties of the obtained solid solutions based on zirconium and hafnium tungstate $M_{1-x}Ln_xW_2O_8$ (M = Zr, Hf; Ln = Eu, Tb, Tm, Lu) are largely determined by the arrangement of WO_4 - tetrahedra, which is influenced by both the secondary recrystallization, as well as the temperature and the partial replacement of Zr^{4+}/Hf^{4+} with Ln^{3+} in the MO_6 – octahedron. The larger Ln^{3+} ions cause more significant WO_4 distortion/disorder at low modifier ion content, x = 0.01, while the smaller ions close to Zr^{4+}/Hf^{4+} size due to their better solubility in the crystal structure, have a stronger influence at the higher content of the modifying ion x = 0.05.

<div align="center">***</div>

The research carried out within the framework of the dissertation extends the knowledge of the properties of zirconium and hafnium tungstate and reveals differences in the properties of solid solutions synthesized on the basis of zirconium and hafnium tungstate. Despite the limited solubility of lanthanide ions in solid solutions, the studies confirm the possibility of controlling some properties of zirconium and hafnium tungstate by modification with lanthanide ions.

V.REFERENCES

1. H.-H. Li, et al. J. Solid State Chem., 180, 2007, 852

2. J. Liao, et al. Materials Research Bulletin, 70, 2015, 7

3. R. D. Shannon. Acta Crystallogr., A, 32, 1976, 751

4. Ch.-Y. Wang, et al. Polyhedron, 159, 2019, 298

5. C. Georgi, H. Kern. Ceram. Int., 35(2), 2009, 755

6. R. Lacomba-Perales, et al. EuroPhys. Letters, 83, 2008, 37002

6. C. Lind, Materials, 5(12), 2012, 1125.

8. D. V. S. Muthu, et al. Solid State Commun., 122 (1–2), 2002, 25.

9. P. Godlewska, et al. J. Alloys Compd., 745, 2018, 779.

10. L. Ouyang, et al. Phys. Rev. B 65, 2002, 113110.

11. J. S. Church, et al. Appl. Catal., 101, 1993, 105

12. D. L. Ferreira, et al. J. Chem. Phys., 147, 2017, 154102

13. U. Kameswari, et al. Int. J. Inorg. Mater. 2, 2000, 333

14. Y. Yamamura, et al. J. Phys. Chem. B 111, 2007, 10118

15. K. Thummavichai, et al. R. Soc. Open Sci. 5, 2018, 171932

16. Y. Yamamura, et al. Phys. Rev. B 66, 2002, 014301

17. J. D. Jorgensen, et al. J. Appl. Phys. 89, 2001, 3184–3188

18. B. Chen, et al. Phys. Rev. B 64, 2001, 214111

20. E. D. Encheva, et al. Bulg. Chem. Comm. Spec. Issue F 50, 2018, 143

21. J. D. Jorgensen, et al. Phys. Rev. B 59, 1999, 215

22. T. Hashimoto, et al. Solid State Commun. 116, 2000, 129

23. E. I. Ross-Medgaarden, et al. Phys. Chem. C, 111, 2007, 15089

24. J. Tauc, et al. J. Phys. Status Solidi B 15, 1966, 627–637

VI. PUBLICATIONS AND REPORTS AT SCIENTIFIC FORUMS

VI.1. Publications related to the dissertation

P.1. E. Encheva, **M. Nedyalkov**, M. Tsvetkov, M. Milanova, The influence of the modification of zirconium tungstate with Eu(III) on the α→β phase transition temperature and optical band gap, Bulg. Chem. Comm., 50 (Special Issue F), 2018, 143-149

P.2. M. Tsvetkov, **M. Nedyalkov**, E. Valcheva, M. Milanova, Characterization of Tungstates of the Type Hf1−xLnxW2O8−x/2 (Ln = Eu, Tm, Lu) Synthesized Using the Hydrothermal Method, Crystals, 2022, 12(3), 327, https://doi.org/10.3390/cryst12030327.

Publication not included in the dissertation

M. Tsvetkov, J. Zaharieva, G. Issa, Z. Cherkezova-Zheleva, **M. Nedyalkov**, D. Paneva, T. Tsoncheva, M. Milanova, Cobalt ferrite modified with Hf(IV), as catalyst for oxidation of ethyl acetate, Catalysis Today, 357, 2020, 541-546, DOI: 10.1016/j.cattod.2019.06.007

VI.2. Presentations at scientific forums related to the topic of the dissertation

D1. Martin Nedyalkov, E. Encheva, M. Tsvetkov, M. Milanova: "The influence of the modifying Eu(III) on the α→β phase transition temperature of zirconium tungstate". Poster report: VII-th National Crystallographic Symposium NCS2018 with international participation, 03-05.10 2018, Sofia, Bulgaria.

D2. Martin Nedyalkov, E. Encheva, M. Tsvetkov, M. Milanova, "Influence of the modification of zirconium tungstate with Eu(III) on the α→β phase transition". Oral Report: Scientific Session 2018 "Chemistry Night", Faculty of Chemistry and Pharmacy, 23.11. 2018, Sofia, Bulgaria

D3. Martin Nedyalkov, M. Tsvetkov, M. Milanova, "Determining the temperature of the α→β phase transition of zirconium tungstate modified with Tb(III) ions". Oral presentation: XVIII National Chemistry Conference for Undergraduates and PhD Students. 15-17.05. 2019, Sofia, Bulgaria

D4. Martin Nedyalkov, M. Tsvetkov, M. Milanova "Tungstates of the Type $Hf_{1-x}Ln_xW_2O_8$, (Ln = Eu, Tm, Lu) studied by High Temperature X-Ray Diffraction". Poster report: 5th ENEFM2019, International International congress on Energy Efficiency and Energy related materials, 22-28.10.2019, Oludeniz, Turkey.